

# Understanding angular momentum transport in red giants: the case of KIC 7341231

T. Ceillier<sup>1</sup>, P. Eggenberger<sup>2</sup>, R. A. García<sup>1</sup>, and S. Mathis<sup>1</sup>

<sup>1</sup> Laboratoire AIM Paris-Saclay, CEA/DSM/IRFU/Sap - CNRS - Université Paris Diderot, Centre de Saclay, F-91191 Gif-sur-Yvette Cedex, France

<sup>2</sup> Observatoire de Genève, Université de Genève, 51 chemin des Maillettes, CH-1290, Sauverny, Suisse

Submitted 14 March 2013, Accepted 22 May 2013

## ABSTRACT

*Context.* Thanks to recent asteroseismic observations, it has been possible to infer the radial differential rotation profile of subgiants and red giants.

*Aims.* We want to reproduce through modeling the observed rotation profile of the early red giant KIC 7341231 and constrain the physical mechanisms responsible for angular momentum transport in stellar interiors.

*Methods.* We compute models of KIC 7341231 including a treatment of shellular rotation and we compare the rotation profiles obtained with the one derived by Deheuvels et al. (2012). We then modify some modeling parameters in order to quantify their effect on the obtained rotation profile. Moreover, we mimic a powerful angular momentum transport during the Main Sequence and study its effect on the evolution of the rotation profile during the subgiant and red giant phases.

*Results.* We show that meridional circulation and shear mixing alone produce a rotation profile for KIC 7341231 too steep compared to the observed one. An additional mechanism is then needed to increase the internal transport of angular momentum. We find that this undetermined mechanism has to be efficient not only during the Main Sequence but also during the much quicker subgiant phase. Moreover, we point out the importance of studying the whole rotational history of a star in order to explain its rotation profile during the red giant evolution.

**Key words.** stars: rotation – stars: oscillations – stars: evolution

## 1. Introduction

Stellar evolution is a very complex process which is not yet fully understood. It is driven by many different physical mechanisms among which rotation is known to be playing a very important part (e.g. Eggenberger et al. 2010b; Maeder 2009; Pinsonneault et al. 1990). The transport of chemical elements and angular momentum by the large-scale meridional circulation and shear mixing, both induced by rotation, can strongly modify the global evolution of a star (Maeder & Zahn 1998; Mathis & Zahn 2004; Zahn 1992). That is why this transport has been included in stellar evolution codes. This implementation follows the shellular rotation hypothesis, which assumes that a strong horizontal turbulent transport in stably stratified stellar radiation zones leads to an angular velocity constant on the isobars and thus depending almost only on the radius (Decressin et al. 2009; Meynet & Maeder 2000). In order to validate these models, it is now necessary to compare their results to observations.

The first constraints that can be used to evaluate the efficiency of rotational mixing in stars are the surface abundances. The influence of rotation has indeed been studied on light elements abundances (e.g. Pinsonneault 2010) and on the evolution of the lithium depletion (e.g. Eggenberger et al. 2012a). The fact that the models including shellular rotation are unable to reproduce lithium abundance in certain cases (Talon & Charbonnel 2003) is a first clue that an additional physical process is at work in the internal layers of low-mass stars (Charbonnel & Talon 2005).

Another way to compare the results of modeling on angular momentum transport with reality is to look directly at observations of rotation in stars. The more straightforward way of doing so is to study measurements of surface rotation. Such studies tend to show that young solar-type stars in rapid rotation would demonstrate a solid-body rotation (see for instance Denissenkov et al. 2010), sign of a strong coupling between the core and the envelope which is not accounted for by meridional circulation and shear mixing alone (Eggenberger et al. 2010a). This is yet another indication that models are missing another transport and mixing process.

One can then go deeper into stars by means of helio- and asteroseismology. The study of stellar oscillations is indeed used to probe their internal layers. As for the Sun, the vast amount of seismological observations have allowed to derive its rotation profile from the surface to the most inner parts (e.g. Elsworth et al. 1995; García et al. 2007; Mathur et al. 2008; Thompson et al. 1996). The resulting profile is almost flat down to  $0.2 R_{\odot}$ , while solar models tend to produce a steeper profile (e.g. Pinsonneault et al. 1989; Turck-Chièze et al. 2010), showing once again the need for an additional coupling process.

To this day, two possible mechanisms have been investigated. The first one implies fossil magnetic fields trapped during the early phases of the star evolution (Braithwaite & Spruit 2004; Duez & Mathis 2010). These magnetic fields are able to transport angular momentum thanks to Maxwell stresses, large-scale torques and magnetic instabilities (e.g. Eggenberger et al. 2005; Garaud & Garaud 2008; Gough & McIntyre 1998; Mathis & Zahn 2005; Strugarek et al. 2011). The second one consists

in internal gravity waves, excited at the limit between the convective and radiative zones. Such waves can indeed transport angular momentum through radiative zones (e.g. Goldreich & Nicholson 1989; Mathis & de Brye 2012; Press 1981; Schatzman 1993; Talon & Charbonnel 2005; Zahn et al. 1997).

The launch of space missions such as CoRoT (Baglin et al. 2006) and *Kepler* (Borucki et al. 2010) have given access to long high-precision light curves for a huge number of stars. Many of these stars exhibit solar-like oscillations at different evolutionary stages, from the main sequence (see for instance Appourchaux et al. 2008; Ballot et al. 2011; Chaplin et al. 2011; García et al. 2009; Mathur et al. 2013; Metcalfe et al. 2012) to more advanced stages such as subgiants (Campante et al. 2011; Mathur et al. 2011, among others) and red giants (e.g. Bedding et al. 2010; Di Mauro et al. 2011; Huber et al. 2011; Mosser et al. 2010, 2012) which allowed to probe stellar interiors. Moreover, the length of the time series available is key to study the dynamics of stars. The existence of surface magnetic activity, for instance, has made possible to constrain the surface rotation (Fröhlich et al. 2012; Mathur et al. 2010) as well as to measure activity cycles (García et al. 2010).

Furthermore, the precise analysis of the rotational splittings of the oscillations modes can strongly constrain the internal rotation profile of main sequence stars (Ballot et al. 2011), young red giants (Deheuvels et al. 2012) and evolved red giants (Beck et al. 2012; Mosser et al. 2012). These splittings have in particular been precisely determined for the red giant KIC 8366239 by Beck et al. (2012). Eggenberger et al. (2012b) and Marques et al. (2013) have shown that models including shellular rotation predict a steep rotation profile which is incompatible with the measured splittings. Eggenberger et al. (2012b) also demonstrated that the asteroseismic measurements strongly constrain the efficiency of the needed additional mechanism for the angular momentum transport.

In this work, we study the case of KIC 7341231, a low-mass and low-metallicity halo early red giant. The very fine observations of this star by *Kepler* have allowed the precise measurement of rotational splittings of mixed modes by Deheuvels et al. (2012) who were able to constrain radial rotation profile of this star by deriving the core's rotation rate and an upper limit of its surface's. In the present paper we present a modeling of KIC 7341231 in order to compare the modeled radial rotation profile with the observed one. In Section 2, we present the known characteristics of KIC 7341231. We then detail the way we modeled the star and discuss our first results in Section 3, while the influence of varying various parameters of the model on the obtained radial differential profile is studied in Section 4. Section 5 then presents the modifications of the modelling in order to mimic a strong angular momentum transport on the Main Sequence and their consequences on the rotation deduced and in Section 6 we focus on the subgiant evolution and the different angular momentum transports during this phase. Finally, our conclusions are given in Section 7.

## 2. Modeled star: KIC 7341231

KIC 7341231, also known as HIP 92775 and G205-42, is an early red giant with a mass of about  $0.84 M_{\odot}$ . Its *Kepler* magnitude is 9.910. It has an effective temperature comprised between 5470 K (Casagrande et al. 2010) and 5483 K (Ammons et al. 2006) and a  $\log g$  between 3.55 (Deheuvels et al. 2012) and 4.06 (Molenda-Zakowicz et al. 2008). Its metallicity [Fe/H] is very low and ranges from  $-2.18$  (Laird et al. 1988) to  $-0.79$  (Ammons et al. 2006). This low metallicity combined with its

high proper motion (39.18 mas/yr in RA and 255.25 in DEC according to van Leeuwen 2007) and its high radial velocity ( $-269.16 \text{ km}\cdot\text{s}^{-1}$ , Latham et al. 2002) indicate that KIC 7341231 is a halo star. All these characteristics are summarised in Table 1.

The radial rotation profile of KIC 7341231 has been derived by Deheuvels et al. (2012). They used a *Kepler* short-cadence photometric light curve of a year long, corrected following the procedures described by García et al. (2011). Their analyse of this light curve resulted first in obtaining the values of the global seismic parameters: a large separation of  $\Delta\nu = 28.9 \pm 0.2 \mu\text{Hz}$  and a period spacing (for dipole g-modes) of  $\Delta\Pi_1 = 107.1 \pm 2.3 \text{ s}$ . They then measured 40 individual eigenmodes of both acoustic and mixed natures, making possible to study the individual rotational splittings of these modes. It allowed them to derive the core's rotation rate and an upper limit for the surface's rotation rate and thus to constrain the radial rotation profile of the star. Deheuvels et al. (2012) have shown that the core of KIC 7341231 is rotating at a frequency  $\Omega_c = 710 \pm 51 \text{ nHz}$  (averaged on the innermost 1.4% of the stellar radius, corresponding to 17% of the total mass) while its surface rotates at a much slower rate  $\Omega_s < 150 \pm 19 \text{ nHz}$ . These properties are summarised in Table 2.

KIC 7341231 has then a much lower mass and a much lower metallicity than the red giant KIC 8366239 observed by Beck et al. (2012), which has a mass of about  $1.5 M_{\odot}$  and a solar metallicity. It is then particularly interesting to compare the rotation profile of KIC 7341231 inferred by observations and the ones predicted by theoretical models to investigate if the conclusions of Eggenberger et al. (2012b) on KIC 8366239 about the efficiency of the internal transport of angular momentum in red giants are still valid for a low-mass, low-metallicity red giant like KIC 7341231, located near the base of the red giant branch.

## 3. Modeling and first results

In order to compute models of KIC 7341231, we use the *Geneva stellar evolution code* (Eggenberger et al. 2008) in which the effects of shellular rotation and the associated meridional circulation and turbulence on stellar evolution have been implemented (Eggenberger et al. 2010b). In this work, we do not consider internal gravity waves or magnetic fields (e.g. Mathis & Zahn 2005; Talon & Charbonnel 2005). All computed models start at the Zero Age Main Sequence (ZAMS). We assume a metallicity [Fe/H] =  $-1$  dex and an initial helium abundance  $Y_{\text{ini}} = 0.260$ . The stop point we select for the computed models corresponds to when the models' asymptotic value of the large separation

$$\Delta\nu = \left( 2 \int_0^R \frac{dr}{c} \right)^{-1}, \quad (1)$$

where  $c$  is the sound speed, is equal to the observed one – without computing surface corrections. We then compare the models' asymptotic value of the period spacing

$$\Delta\Pi_1 = \frac{\pi}{\sqrt{2}} \left( \int_{r_1}^{r_2} \frac{N}{r} dr \right)^{-1}, \quad (2)$$

where  $N$  is the Brunt-Väisälä frequency and  $N(r) > 0$  for  $r_1 < r < r_2$ , to verify that it has the same value as the observed one. In order to best reproduce the observed surface rotation, we focus on models with a low initial rotational velocity on the ZAMS of  $v_{\text{ini}} = 2 \text{ km}\cdot\text{s}^{-1}$ .

In accordance with Deheuvels et al. (2012), we find that a model with a mass  $M = 0.84 M_{\odot}$  reproduces both the observed large separation and period spacing at the same age

**Table 1.** Observational characteristics of KIC 7341231.

Observables	Values	Sources
$T_{\text{eff}}$	$5470 \pm 30$ K	Casagrande et al. 2010
	$5483 \pm 60$ K	Ammons et al. 2006
$\log g$	$3.55 \pm 0.03$	Deheuvels et al. 2012
	$4.06 \pm 0.29$	Molenda-Żakowicz et al. 2008
[Fe/H]	$-2.18 \pm 0.06$ dex	Laird et al. 1988
	$-0.79 \pm 0.14$ dex	Ammons et al. 2006
Proper motion	$39.18 \pm 0.85$ mas $\cdot$ yr $^{-1}$ (RA)	van Leeuwen 2007
	$255.55 \pm 1.24$ mas $\cdot$ yr $^{-1}$ (DEC)	
Radial velocity	$-269.16 \pm 0.14$ km $\cdot$ s $^{-1}$	Latham et al. 2002

**Table 2.** Seismically derived properties of KIC 7341231 (Deheuvels et al. 2012).

Quantities	Values
$\Delta\nu$	$28.9 \pm 0.2$ $\mu$ Hz
$\Delta\Pi_1$	$112.8 \pm 0.3$ s
$\Omega_c$	$710 \pm 51$ nHz
$\Omega_s$	$< 150 \pm 19$ nHz

**Table 3.** Characteristics of the computed models.

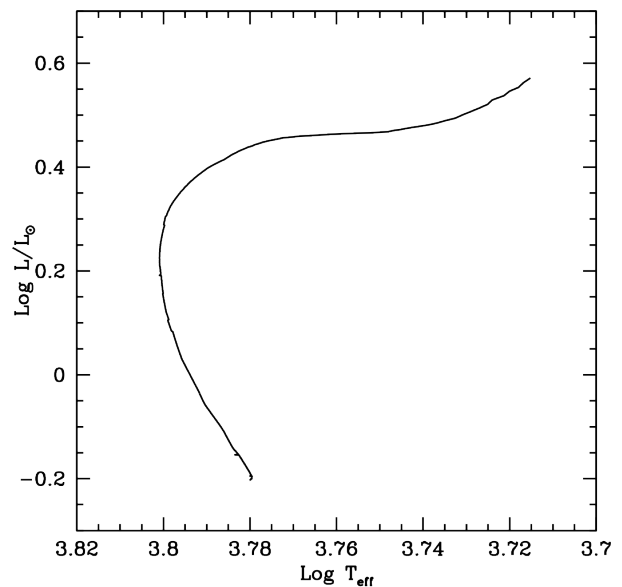
Quantities	Values
[Fe/H]	-1 dex
$Y_{\text{ini}}$	0.260
$v_{\text{ini}}$	2 km $\cdot$ s $^{-1}$
$M$	$0.84 \pm 0.01 M_{\odot}$
Age	$13.01 \pm 0.06$ Gyr
$\Delta\nu$	$30 \pm 4$ $\mu$ Hz
$\Delta\Pi_1$	$115 \pm 9$ s
$\Omega_c$	$33 \pm 6$ $\mu$ Hz
$\Omega_s$	$36 \pm 10$ nHz

$T = 13.01$  Gyr. The characteristics of this model are recalled in Table 3. Its evolutionary track (Figure 1 and Figure 2) shows that KIC 7341231 is an early red giant that has recently finished the subgiant phase.

We find that the obtained radial differential rotation profile is much steeper than the observed one, as can be seen in Figure 3: the rotation rate of the core is almost two orders of magnitude higher than the observed value (33  $\mu$ Hz for the model versus 0.71  $\mu$ Hz for the observations). This is in complete agreement with the results obtained by Eggenberger et al. (2012b) for the more massive star KIC 8366239, by Pinsonneault et al. (1989) and Turck-Chièze et al. (2010) for the Sun and also by Marques et al. (2013) for a 1.3  $M_{\odot}$  star. It shows that, for a low-mass and low-metallicity red giant like KIC 7341231, the shellular rotation and the subsequent meridional circulation and shear mixing alone produce an internal coupling insufficient to explain the observed rotation profile.

#### 4. Influence of modeling parameters

In order to investigate the effects of varying different modeling parameters on the rotation profile we compute models with the same global properties (mass,  $v_{\text{ini}}$ , metallicity...) but with modified properties (see also Marques et al. 2013). We study the influence of the magnetic braking during the main sequence, the atomic diffusion, the value of the mixing-length parameter, the value of initial helium abundance and the metallicity. The re-


**Fig. 1.** Evolutionary track of the 0.84  $M_{\odot}$  model from the ZAMS, including the effects of rotation. The end point corresponds to the selected model of the star, matching both the observed large separation and period spacing.

sulting characteristics of these modified models are summarised in Table 4. The reasons why these parameters were chosen are detailed in the following paragraphs.

We first wanted to study the influence of magnetic braking on the modeled rotation profile, as it modifies directly the surface rotation of the star. Hence, switching on the magnetic braking during the main sequence reduces the surface rotation rate which amplifies the radial differential rotation and thus modifies the structure of the star and increases the strength of the meridional circulation.

We then investigated the effect of atomic diffusion – or microscopic diffusion – on the rotation profile. To calculate the reference model, we had taken into account only transport mechanisms linked to the rotation, while here we add atomic diffusion to these transport mechanisms. This would modify the transport of chemicals in the star, changing its structure and thus, indirectly, the angular momentum transport.

A parameter that is often fixed to a solar value in stellar models is the mixing length parameter  $\alpha_{\text{MLT}}$ . It is however very difficult to be sure that this parameter can be set to the same value for a whole range of different stars. Indeed, when modeling red giants, one can wonder if the vast differences between the Sun's and red giants' structures cannot prevent us from using the solar

**Table 4.** Characteristics of the modified models.

Model #	Modified parameter	Reference value	Modified value	Age (Gyr)	$\Delta\nu$ ( $\mu\text{Hz}$ )	$\Delta\Pi_1$ (s)
1	Magnetic braking	Off	On	$12.97 \pm 0.09$	$34 \pm 5$	$122 \pm 10$
2	Atomic diffusion	Off	On	$12.65 \pm 0.09$	$32 \pm 5$	$119 \pm 10$
3	$\alpha_{\text{MLT}}$	1.6	1.7	$12.97 \pm 0.09$	$34 \pm 6$	$121 \pm 10$
4	$Y_{\text{ini}}$	0.26	0.3	$9.71 \pm 0.07$	$33 \pm 6$	$123 \pm 12$
5	[Fe/H]	-1	-0.8	$14.16 \pm 0.08$	$31 \pm 5$	$116 \pm 8$

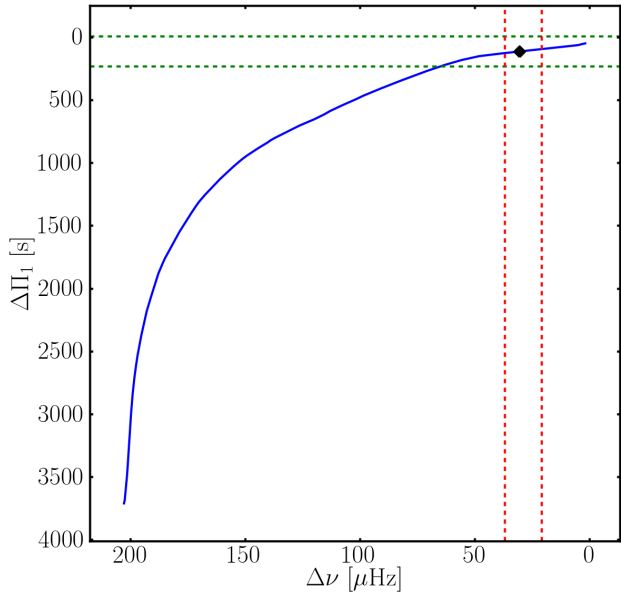


**Fig. 2.** Evolutionary track of the  $0.84 M_{\odot}$  model in the asteroseismic H.-R. diagram (blue). The black diamond indicates the position of the selected model. The dashed red and green lines correspond to the errors bars on the observed large separation and period spacing, respectively, from Deheuvels et al. (2012). These error bars have been magnified 40 times for the large separation and 400 times for the period spacing in order to be visible.

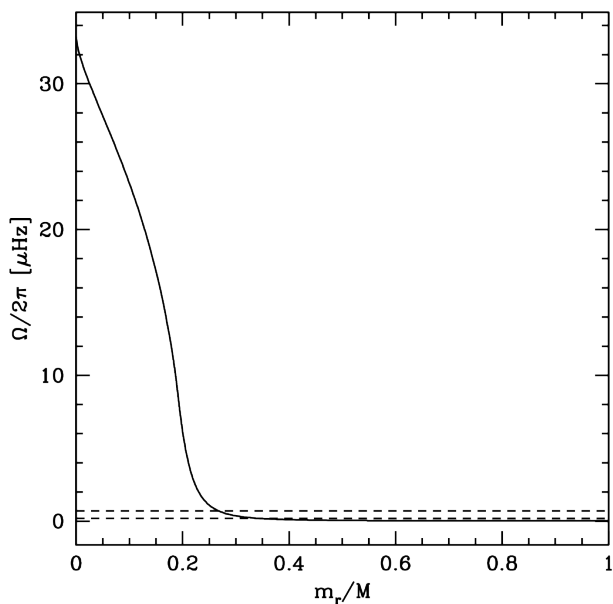


**Fig. 3.** Rotation profile of the selected model at the end of the evolutionary track (solid line). The two dashed lines correspond to the core and the surface rotation rates derived by Deheuvels et al. (2012).

**Table 5.** Modifications of the rotation rates of the modified models.

Model #	Change for $\Omega_c$	Change for $\Omega_s$
1	-9 %	+8 %
2	-5 %	+8 %
3	-8 %	+19 %
4	-18 %	+5 %
5	+2 %	+5 %

value. That is why we wanted to see the effect of a change in  $\alpha_{\text{MLT}}$ . We thus calculated a model similar to the reference one in every aspects except for the mixing-length parameter that we set to 1.7 instead of 1.6. The extension of the convective zone being increased by this change, the distribution of angular momentum should be altered as well.

As a halo star, KIC 7341231 is assumed to have a low initial helium abundance. It is however difficult to have a precise estimate of its value. In order to evaluate the influence of this quantity on the internal differential rotation profile, we calculated a model with a slightly higher  $Y_{\text{ini}}$ : 0.3 instead of 0.26. This model would correspond to a star born later than KIC 7341231 and could show the differences in angular momentum transport between two stars formed at two different epochs. This change has also a strong influence on the age of the model, which is 9.71 Gyr. While this difference with the reference model is logical, it is resulting in a higher luminosity and a slightly higher  $\log g$ .

For the same reasons why KIC 7341231 is assumed to have a low initial helium abundance, it is also assumed to have a very low metallicity. Once again, it remains quite difficult to estimate accurately this quantity. That is why we decided to assess the influence of the metallicity on the obtained rotation profile. To do so, we computed a model with a metallicity of [Fe/H] = -0.8 (in accordance with Ammons et al. 2006) instead of -1. Like the helium-richer model, this metal-richer model would correspond to a star formed later than KIC 7341231. Here again, the age of the model is strongly modified: 14.16 Gyr, far from the 13.01 Gyr of the reference model. This leads to a higher effective temperature, a lower luminosity and a slightly more elevated  $\log g$ .

All these modifications are bound to influence the structure and evolution of the modeled star, thus resulting in different values of the large separation and period spacing. Nevertheless, these changes are relatively small and the obtained values are always compatible with the observed ones, as can be seen in Table 4.

The changes implied in the rotation profile are however more significant. In Figure 4, we show the difference between the rotation profiles of the modified models and the reference model's one. The modifications of the core rotation rate and the surface rotation rate are also summarised in Table 5. It is then clear that modifying the modeling parameters induces small changes in the rotation profile compared to the gap between the modeled

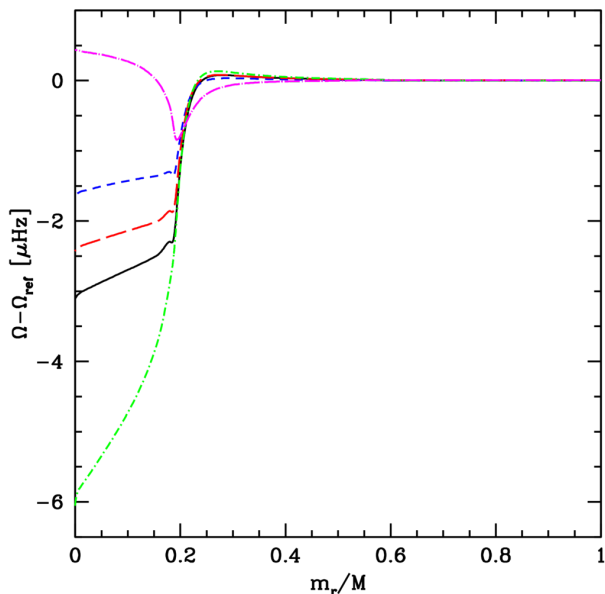


**Fig. 4.** Differences between the rotation profiles of the modified models and the rotation profile of the reference model. Black, solid: Model 1 (Magnetic braking On). Blue, short-dashed: Model 2 (Atomic diffusion On). Red, long-dashed: Model 3 (modified  $\alpha_{\text{MLT}}$ ). Green, dot-short-dashed: Model 4 (modified  $Y_{\text{ini}}$ ). Magenta, dot-long-dashed: Model 5 (modified  $[\text{Fe}/\text{H}]$ ).

and observed core rotation rates. We are still far from reproducing the relatively flat rotation profile deduced from asteroseismic measurements. Once again, this suggests that another and yet undetermined physical process is at work in stellar interiors to increase angular momentum transport, in addition to meridional circulation and shear mixing.

For the time being, it would seem that the two best candidates for angular momentum transport from the core to the more external layers are internal gravity waves excited by the turbulent convective envelope (Mathis 2009; Schatzman 1993; Talon & Charbonnel 2005, 2008; Zahn et al. 1997) and fossil magnetic field with related MHD processes (Eggenberger et al. 2005; Gough & McIntyre 1998; Mathis & Zahn 2005; Spada et al. 2010; Strugarek et al. 2011; Zahn et al. 2007). These two processes would tend to damp the differential rotation gradient inside stars and might explain the internal rotation profile of the Sun and red giants.

## 5. Simulating a strong angular momentum transport on the Main Sequence

It is then clear that another process is needed to account for the important angular momentum transport in stellar interiors. While it is still unclear what this process is precisely but we wanted to study the possible effects of such a process on the rotation profile of the early red giant KIC 7341231. What we know is that this mechanism would flatten the rotation profile of the star. As the longest evolutionary phase in stellar life is the main sequence, the unknown process would probably strongly impact the rotation profile of the star during this phase. Following this hypothesis, we decided to consider an extreme case, corresponding to a complete homogenisation of angular momentum during the main sequence. This homogenisation is indeed similar to the effects of a very strong and highly efficient angular momentum

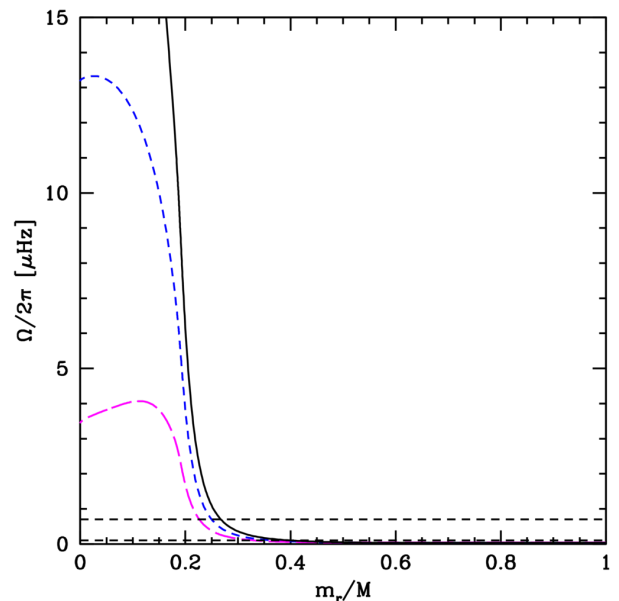


**Fig. 5.** Rotational profiles of the models with and without solid-body rotation during the main sequence. Black: same as Fig. 3. Blue, short-dashed: model with solid-body rotation until  $X_c = 0.1$ . Magenta, long-dashed: model with solid-body rotation until  $X_c = 0$ .

transport mechanism. The efficiency of such an additional process being unknown on smaller timescales such as the subgiant phase, we decided to let the star evolve normally as soon as the end of the main sequence. We are well aware that this approach is slightly crude and that the real effects of an additional phenomenon would be more subtle but we chose this methodology as an extreme case, in order to put constraints on the aforementioned process and have a first quantitative evaluation of such a process.

In order to simulate a strong homogenizing mechanism, we therefore forced in the evolution code a solid-body rotation of the star during the main sequence, allowing the transport of angular momentum through meridional circulation and shear mixing only during the post-main sequence evolution. The initial rotational velocity on the ZAMS was still fixed at  $v_{\text{ini}} = 2 \text{ km} \cdot \text{s}^{-1}$ . We have computed two such models: for the first one the solid-body rotation is maintained until the hydrogen abundance in the core reaches  $X_c = 0.1$ , while for the second it stops when there is no more hydrogen in the core. The first case does not correspond to the exact end of the main sequence but allowed us to observe the influence of the rotation of the star during the main sequence on the red giant's rotation profile. The resulting rotation profiles (Figure 5) were much less steep than previously, as could be expected. Without surprise, the later we switch off the solid-body rotation, the flatter the rotation profile. This shows the sensitivity of the red giant rotation profile to the efficiency of the angular momentum transport during the main sequence. Nevertheless, the gap is still huge between what we obtain and what is observed: the models' core rotation rates are at least one order of magnitude higher than the observed one ( $\Omega_c = 3.5$  and  $13.2 \mu\text{Hz}$  for models versus  $0.71 \mu\text{Hz}$  for observations). This suggests that the required process, whatever what it might be, has to be efficient also on small time scales such as the subgiant evolution.

Another remarkable consequence of the solid-body rotation during the main sequence is that even in the later evolution of

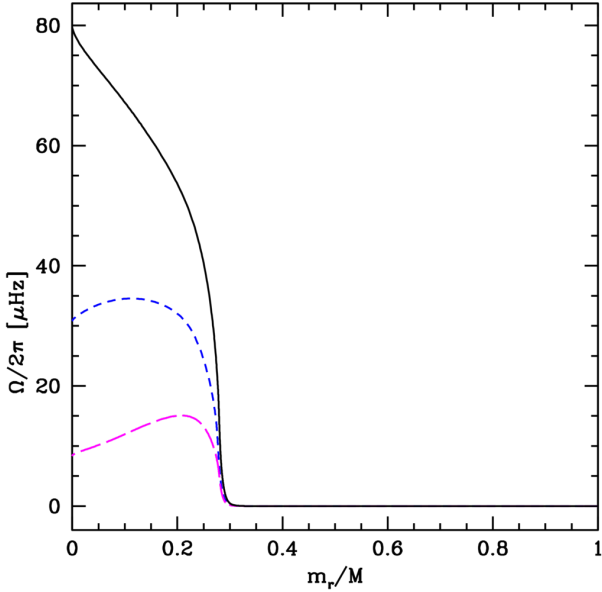


**Fig. 6.** Rotational profiles of the models with and without solid-body rotation during the main sequence, but after the subgiant phase (at an age  $T = 13.40$  Gyr). Black: normal case (no solid-body rotation). Blue, short-dashed: model with solid-body rotation until  $X_c = 0.1$ . Magenta, long-dashed: model with solid-body rotation until  $X_c = 0$ .

the star (i.e. the red giant phase) the rotation profiles obtained strongly differ from the one corresponding to the normal case (i.e. without solid-body rotation). This discrepancy can be seen in Figure 6. In particular, we can observe a decrease of the rotational rate in the core of the star, which was already visible in Figure 5 but less prominent. This shows that, in these models, the rotational history of the star is not completely erased by its evolution during the subgiant and red giant phases. In order to fully understand red giants' rotation profiles it is thus adamant to study the evolution of the rotation inside the star during its whole evolution.

## 6. Subgiant evolution and angular momentum transport

We have seen that the missing angular momentum transport mechanism has to be efficient during the short-lived subgiant phase. But what of the transport processes already considered? In order to quantify their effect during this phase, we compared the evolution of the rotational profile during the subgiant phase in two different cases. For the first one, we took into account rotationally induced processes such as meridional circulation and shear mixing. For the second one, we considered only angular momentum conservation. Thus the difference between the obtained rotational profiles at the end of the subgiant phase is a good proxy of the efficiency of the transport processes.

This has been done for the reference model and for the model with solid-body rotation during the main sequence until  $X_c = 0.1$ . The resulting profiles are shown in Figures 7 and 8. While considering rotationally induced transport reduces indeed the core's rotation rate, the effect is of very small magnitude ( $1.5 \mu\text{Hz}$  maximum compared to  $\Omega_c = 33 \mu\text{Hz}$ , a 4.5% change). The evolution of the star's rotation profile during subgiant evolution is therefore completely dominated by the sheer conservation

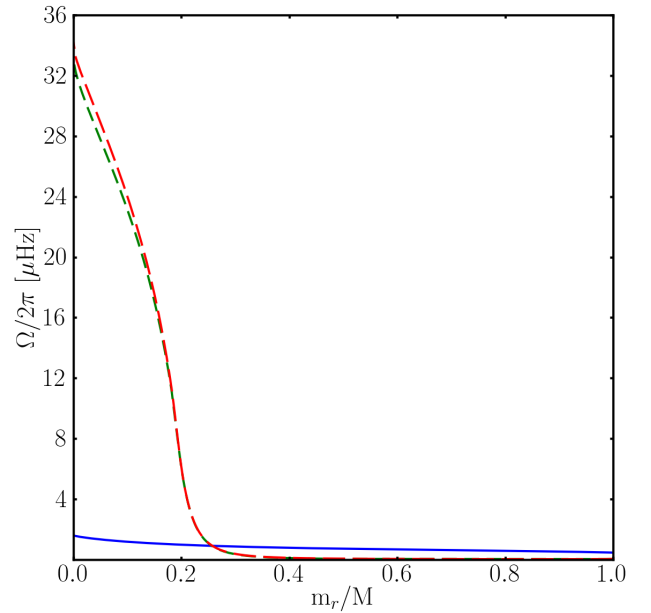


**Fig. 7.** Rotational profiles of the reference model at different evolution times. Blue, solid: end of Main Sequence. Green, short-dashed: end of Subgiant evolution considering all angular momentum transport phenomena. Red, long-dashed: end of subgiant evolution considering only conservation of angular momentum during the subgiant phase.

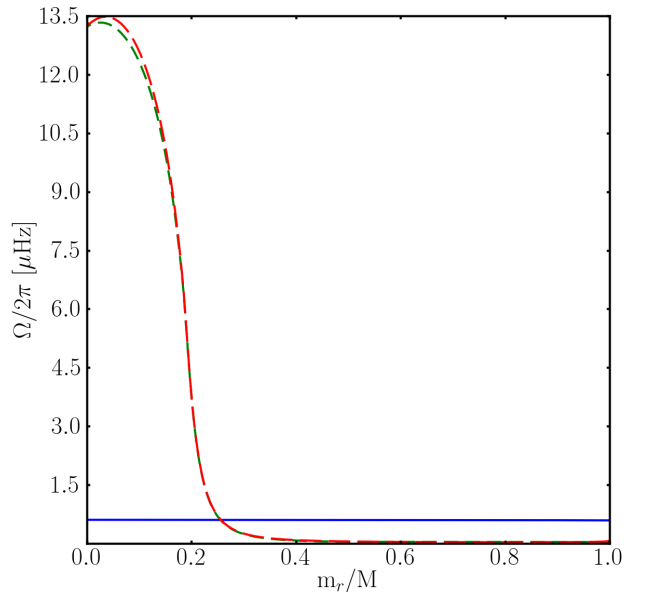


**Fig. 8.** Rotational profiles of the model with solid-body rotation during Main Sequence (until  $X_c = 0.1$ ) at different evolution times. Colors: same as Figure 7.

of angular momentum due to the profound modifications of the star's structure.

This comparison emphasizes that any angular momentum transport phenomenon considered must be considerably more efficient than meridional circulation and shear mixing on small timescales. More precisely, during the subgiant phase, this phenomenon has to be strong enough to counterbalance angular momentum conservation. Once again, this is a rather important constraint for the studied additional processes such as internal gravity waves and magnetic fields.

## 7. Conclusion

The comparison between the radial rotation profile of the red giant KIC 7341231 inferred from asteroseismic measurements with profiles predicted by stellar models – including shellular rotation, meridional circulation and shear mixing – have shown that such models are unable to reproduce the observed internal rotational rates. The theoretical rotation profiles are indeed too steep compared to the one deduced from observations: in the case of KIC 7341231 the model's core is rotating at least 30 times faster than what has been deduced through asteroseismic means. This is in perfect agreement with the conclusions of Eggenberger et al. (2012b), Marques et al. (2013) and Ceillier et al. (2012) and shows that this discrepancy is also found for a low-mass, low-metallicity red giant like KIC 7341231 (see also Palacios et al. 2006).

These results illustrate the need to progress in our understanding and modeling of (magneto-)hydrodynamical processes at work in stellar interiors and to implement new physical processes into stellar evolution codes, such as internal gravity waves or magnetic fields. We have demonstrated here that these processes, however efficient during the long-lasting main sequence, have to be very effective during the rapid evolution of the subgiant phase. Furthermore, we have also shown that their effect on internal rotation must be considered over the whole evolution of the star and that the rapid evolution during the subgiant phase does not completely erase all the previous rotational history of the star.

It would be interesting to determine the efficiency of the unknown physical process needed for the internal transport of angular momentum in order to correctly reproduce the observed rotation profile of KIC 7341231. This would allow a comparison with the effective viscosity of  $3 \cdot 10^4 \text{ cm}^2 \text{ s}^{-1}$  found for the more massive red giant KIC 8366239 (Eggenberger et al. 2012b), although we would like to remind the reader that neither internal gravity waves nor fossil magnetic fields have an effect comparable with an effective viscosity (see Mathis 2013).

We have no doubt that codes in which the effects on angular momentum transport of processes like internal gravity waves or magnetic fields have been implemented will allow us to understand more accurately the various physical mechanisms at work in stars. In such improvement of our vision of the dynamical evolution of stars, asteroseismology is then one of the most promising ways to get strong constraints as demonstrated here with the case of KIC 7341231.

*Acknowledgements.* TC, RAG and SM acknowledge the CNES support of CoRoT and of asteroseismic activities at the SAP – CEA/Saclay and the CNRS/INSU PNPS support. TC and SM thank the Geneva Observatory for its hospitality. PE was partly supported by the Swiss National Science Foundation. The authors would like to thank the referee for her/his suggestions which helped improving the paper.

## References

Ammons, S. M., Robinson, S. E., Strader, J., et al. 2006, *The Astrophysical Journal*, 638, 1004  
 Appourchaux, T., Michel, E., Auvergne, M., et al. 2008, *Astronomy and Astrophysics*, 488, 705  
 Baglin, A., Auvergne, M., Barge, P., et al. 2006, in *ESA Special Publication*, Vol. 1306, *ESA Special Publication*, ed. M. Fridlund, A. Baglin, J. Lochard, & L. Conroy, 33  
 Ballot, J., Gizon, L., Samadi, R., et al. 2011, *Astronomy & Astrophysics*, 530, A97  
 Beck, P. G., Montalbán, J., Kallinger, T., et al. 2012, *Nature*, 481, 55  
 Bedding, T. R., Huber, D., Stello, D., et al. 2010, *The Astrophysical Journal*, 713, L176

Borucki, W. J., Koch, D., Basri, G., et al. 2010, *Science*, 327, 977  
 Braithwaite, J. & Spruit, H. C. 2004, *Nature*, 431, 819  
 Campante, T. L., Handberg, R., Mathur, S., et al. 2011, *Astronomy & Astrophysics*, 534, A6  
 Casagrande, L., Ramírez, I., Meléndez, J., Bessell, M., & Asplund, M. 2010, *Astronomy and Astrophysics*, 512, A54  
 Ceillier, T., Eggenberger, P., García, R. A., & Mathis, S. 2012, *Astronomische Nachrichten*, 333, 971  
 Chaplin, W. J., Kjeldsen, H., Christensen-Dalsgaard, J., et al. 2011, *Science (New York, N.Y.)*, 332, 213  
 Charbonnel, C. & Talon, S. 2005, *Science (New York, N.Y.)*, 309, 2189  
 Decressin, T., Mathis, S., Palacios, A., et al. 2009, *Astronomy and Astrophysics*, 495, 271  
 Deheuvels, S., García, R. A., Chaplin, W. J., et al. 2012, *The Astrophysical Journal*, 756, 19  
 Denissenkov, P. A., Pinsonneault, M., Terndrup, D. M., & Newsham, G. 2010, *The Astrophysical Journal*, 716, 1269  
 Di Mauro, M. P., Cardini, D., Catanzaro, G., et al. 2011, *Monthly Notices of the Royal Astronomical Society*, 415, 3783  
 Duez, V. & Mathis, S. 2010, *Astronomy and Astrophysics*, 517, A58  
 Eggenberger, P., Haemmerlé, L., Meynet, G., & Maeder, A. 2012a, *Astronomy & Astrophysics*, 539, A70  
 Eggenberger, P., Maeder, A., & Meynet, G. 2005, *Astronomy and Astrophysics*, 440, L9  
 Eggenberger, P., Maeder, A., & Meynet, G. 2010a, *Astronomy and Astrophysics*, 519, L2  
 Eggenberger, P., Meynet, G., Maeder, A., et al. 2008, *Astrophysics and Space Science*, 316, 43  
 Eggenberger, P., Miglio, A., Montalbán, J., et al. 2010b, *Astronomy and Astrophysics*, 509, A72  
 Eggenberger, P., Montalbán, J., & Miglio, A. 2012b, *Astronomy & Astrophysics*, 544, L4  
 Elsworth, Y., Howe, R., Isaak, G. R., et al. 1995, *Nature*, 376, 669  
 Fröhlich, H.-E. E., Frasca, A., Catanzaro, G., et al. 2012, *Astronomy & Astrophysics*, 543, A146  
 Garaud, P. & Garaud, J.-D. 2008, *Monthly Notices of the Royal Astronomical Society*, 391, 1239  
 García, R. A., Hekker, S., Stello, D., et al. 2011, *Monthly Notices of the Royal Astronomical Society: Letters*, 414, L6  
 García, R. A., Mathur, S., Salabert, D., et al. 2010, *Science (New York, N.Y.)*, 329, 1032  
 García, R. A., Régulo, C., Samadi, R., et al. 2009, *Astronomy and Astrophysics*, 506, 41  
 García, R. A., Turck-Chièze, S., Jiménez-Reyes, S. J., et al. 2007, *Science (New York, N.Y.)*, 316, 1591  
 Goldreich, P. & Nicholson, P. D. 1989, *The Astrophysical Journal*, 342, 1079  
 Gough, D. & McIntyre, M. 1998, *Nature*, 394, 755  
 Huber, D., Bedding, T. R., Stello, D., et al. 2011, *The Astrophysical Journal*, 743, 143  
 Laird, J. B., Carney, B. W., & Latham, D. W. 1988, *The Astronomical Journal*, 95, 1843  
 Latham, D. W., Stefanik, R. P., Torres, G., et al. 2002, *The Astronomical Journal*, 124, 1144  
 Maeder, A. 2009, *Physics, Formation and Evolution of Rotating Stars*, *Astronomy and Astrophysics Library* (Berlin, Heidelberg: Springer Berlin Heidelberg)  
 Maeder, A. & Zahn, J.-P. 1998, *Astronomy and Astrophysics*, 334, 1000  
 Marques, J. P., Goupil, M. J., Lebreton, Y., et al. 2013, *Astronomy & Astrophysics*, 549, A74  
 Mathis, S. 2009, *Astronomy and Astrophysics*, 506, 811  
 Mathis, S. 2013, in *Lecture Notes in Physics*, Berlin Springer Verlag, Vol. 865, *Lecture Notes in Physics*, Berlin Springer Verlag, ed. M. Goupil, K. Belkacem, C. Neiner, F. Lignières, & J. J. Green, 23  
 Mathis, S. & de Brye, N. 2012, *Astronomy & Astrophysics*, 540, A37  
 Mathis, S. & Zahn, J.-P. 2004, *Astronomy and Astrophysics*, 425, 229  
 Mathis, S. & Zahn, J.-P. 2005, *Astronomy and Astrophysics*, 440, 653  
 Mathur, S., Eff-Darwich, A., García, R. A., & Turck-Chièze, S. 2008, *Astronomy and Astrophysics*, 484, 517  
 Mathur, S., García, R. A., Catala, C., et al. 2010, *Astronomy and Astrophysics*, 518, A53  
 Mathur, S., García, R. A., Morgenthaler, A., et al. 2013, *Astronomy & Astrophysics*, 550, A32  
 Mathur, S., Handberg, R., Campante, T. L., et al. 2011, *The Astrophysical Journal*, 733, 95  
 Metcalfe, T. S., Chaplin, W. J., Appourchaux, T., et al. 2012, *The Astrophysical Journal*, 748, L10  
 Meynet, G. & Maeder, A. 2000, *Astronomy and Astrophysics*, 361, 101  
 Molenda-Zakowicz, J., Frasca, A., & Latham, D. W. 2008, 13

- Mosser, B., Belkacem, K., Goupil, M.-J. J., et al. 2010, *Astronomy and Astrophysics*, 517, A22
- Mosser, B., Goupil, M. J., Belkacem, K., et al. 2012
- Palacios, A., Charbonnel, C., Talon, S., & Siess, L. 2006, *Astronomy and Astrophysics*, 453, 261
- Pinsonneault, M. H. 2010, *Proceedings of the International Astronomical Union*, 5, 375
- Pinsonneault, M. H., Kawaler, S. D., & Demarque, P. 1990, *The Astrophysical Journal Supplement Series*, 74, 501
- Pinsonneault, M. H., Kawaler, S. D., Sofia, S., & Demarque, P. 1989, *The Astrophysical Journal*, 338, 424
- Press, W. H. 1981, *The Astrophysical Journal*, 245, 286
- Schatzman, E. 1993, *Astronomy & Astrophysics*, 279, 431
- Spada, F., Lanzafame, A. C., & Lanza, A. F. 2010, *Monthly Notices of the Royal Astronomical Society*, 404, 641
- Strugarek, A., Brun, A. S., & Zahn, J.-P. 2011, *Astronomy & Astrophysics*, 532, A34
- Talon, S. & Charbonnel, C. 2003, *Astronomy and Astrophysics*, 405, 1025
- Talon, S. & Charbonnel, C. 2005, *Astronomy and Astrophysics*, 440, 981
- Talon, S. & Charbonnel, C. 2008, *Astronomy and Astrophysics*, 482, 597
- Thompson, M. J., Toomre, J., Anderson, E. R., et al. 1996, *Science*, 272, 1300
- Turck-Chièze, S., Palacios, A., Marques, J. P., & Nghiem, P. A. P. 2010, *The Astrophysical Journal*, 715, 1539
- van Leeuwen, F. 2007, *Astronomy and Astrophysics*, 474, 12
- Zahn, J.-P. 1992, *Astronomy and Astrophysics*, 265, 115
- Zahn, J.-P., Brun, A. S., & Mathis, S. 2007, *Astronomy and Astrophysics*, 474, 145
- Zahn, J.-P., Talon, S., & Matias, J. 1997, *Astronomy and Astrophysics*, 322, 320